Extraction of higher harmonic wave elevation and loads using a four-phase approach in fully nonlinear simulations

***Xingya Feng[a,d], Paul H. Taylor[b], Wei Bai[c], Thomas A. A. Adcock[d]**
[a]Department of Ocean Science and Engineering, Southern University of Science and Technology, China
[b]Faculty of Engineering and Mathematical Sciences, University of Western Australia, Australia
[c] School of Computing, Mathematics and Digital Technology, Manchester Metropolitan University, UK
[d]Department of Engineering Science, University of Oxford, OX1 3PJ, UK
∗fengxy@sustech.edu.cn

1. Introduction

Due to the industry interest of further reducing the cost of offshore wind energy, understanding and accurate prediction of the higher-order nonlinear wave loads on the structure is of great importance in harsh offshore environments. A well-known phenomenon caused by high-frequency loads is the 'ringing'. The 'ringing' is more likely caused by a large single transient event in a random sea rather than a regular wave train. While frequency-domain potential models produce steady-state responses, it might be more practically appropriate to investigate the harmonic wave loading in a transient extreme wave in the time domain. The present work presents time-domain nonlinear simulations of wave-structure interactions and analyzing the characteristics of the higher harmonics of the wave responses and loadings.

Analysis of nonlinear wave loads on a vertical cylinder had been carried out by mainly extending the frequency-domain perturbation analysis to higher orders, for example the FNV model in [2] and the M&M model in [5]. Both the FNV and M&M model show good agreement when the wavenumber is small (long waves). In a separate approach Rainey [6] derived a simplified expression for wave loads up to third order on a slender body in the perspective of fluid kinetic energy. Extension of the perturbation analysis to the fourth and higher orders can be extremely complicated and impractical. Fully nonlinear numerical models ([3, 1]) have been developed to consider higher orders and to deal with structures of variational geometry.

We extend the nonlinear numerical model in [1] to implement the generation of focused wave groups and the phase manipulation technique [4] for extracting the higher harmonics. The technique is demonstrated successful for extraction of higher harmonics from fully nonlinear results. The higher harmonic wave loads are found to have the 'Stokes-type' structure, where harmonic load coefficients (non-dimensionalised force) are almost constant with increasing wave steepness. It will be practically useful for quick estimation of higher harmonic wave loading given the linear load and the harmonic coefficients.

2. Methodology

2.1. Harmonic decomposition model

We utilise a phase-controlled harmonic decomposition method to extract the different harmonics. With the assumption of a relatively narrow-banded spectrum, the focused wave group can be assumed to have a slowly-varying amplitude $A(t)$ near focusing. We write the wave force $F(t)$ in a 'Stokes-type' expanded form with respect to wave steepness (or amplitude for a fixed wavenumber) as

$$\begin{aligned} F(t) = {} & A\mathcal{F}_{11}\cos\varphi + A^2(\mathcal{F}_{20} + \mathcal{F}_{22}\cos 2\varphi) + A^3(\mathcal{F}_{31}\cos\varphi + \mathcal{F}_{33}\cos 3\varphi) \\ & + A^4(\mathcal{F}_{40} + \mathcal{F}_{42}\cos 2\varphi + \mathcal{F}_{44}\cos 4\varphi) + O(A^5) \end{aligned} \tag{1}$$

up to fourth order of the steepness k_pA. The coefficients $\mathcal{F}_{mn}$ represent kernel functions corresponding to sum ($m = n$) and difference ($m - n = 2, 4\ldots$) harmonics and $\varphi = \omega t + \varphi_0$ is the phase of the linear component of the incident wave with φ_0 a prescribed phase. The expression can be rearranged as

$$\begin{aligned} F(t) = {} & A^2\mathcal{F}_{20} + A^4\mathcal{F}_{40} + \left(A\mathcal{F}_{11} + A^3\mathcal{F}_{31}\right)\cos\varphi + \left(A^2\mathcal{F}_{22} + A^4\mathcal{F}_{42}\right)\cos 2\varphi \\ & + A^3\mathcal{F}_{33}\cos 3\varphi + A^4\mathcal{F}_{44}\cos 4\varphi \end{aligned} \tag{2}$$

To separate the different harmonic components $\cos n\varphi$, we use the phase manipulation technique presented in [4] The approach prescribes the phase at which the waves are generated so that four runs are carried out with phases: $\varphi_0 = 0°, 90°, 180°$ and $270°$. By linearly combining the four corresponding responses F_0, F_{90}, F_{180} and F_{270}, the harmonics can be separated as:

$$\left(A\mathcal{F}_{11} + A^3\mathcal{F}_{31}\right)\cos\omega t = (F_0 - F_{90}^H - F_{180} + F_{270}^H)/4, \tag{3a}$$

$$\left(A^2\mathcal{F}_{22} + A^4\mathcal{F}_{42}\right)\cos 2\omega t = (F_0 - F_{90} + F_{180} - F_{270})/4, \tag{3b}$$

$$A^3\mathcal{F}_{33}\cos 3\omega t = (F_0 + F_{90}^H - F_{180} - F_{270}^H)/4, \tag{3c}$$

$$A^2\mathcal{F}_{20} + A^4\mathcal{F}_{40} + A^4\mathcal{F}_{44}\cos 4\omega t = (F_0 + F_{90} + F_{180} + F_{270})/4. \tag{3d}$$

where the superscript H denotes the Hilbert transform of the time signal. Note that the harmonic terms might not be exactly the same order, for instance, Eq. (3a) is the first harmonic term but it contains a 3rd-order difference components $A^3\mathcal{F}_{31}$. This term is two orders smaller than the sum term $A\mathcal{F}_{11}$ thus it is not necessary to further separate them except the term $A^2\mathcal{F}_{20}$ in (3d) which is the second order difference component.

2.2. Fully nonlinear potential model

We extended the potential flow model presented in [1] for regular waves. The model, following the ideal potential flow assumption, solves the velocity potential satisfying the Laplace equation in the time domain. The exact free-surface dynamic and kinematic boundary conditions are satisfied without linearisation. A rectangular Numerical Wave Tank (NWT) is set up in the model, and waves are generated and controlled through the movement of the wavemaker. The boundary value problem is solved numerically in the time domain. A higher-order boundary element method (HOBEM) is employed to formulate the boundary integral equations (BIEs). The Mixed Eulerian-Lagrangian (MEL) algorithm is adopted to update the nonlinear free surface during time marching.

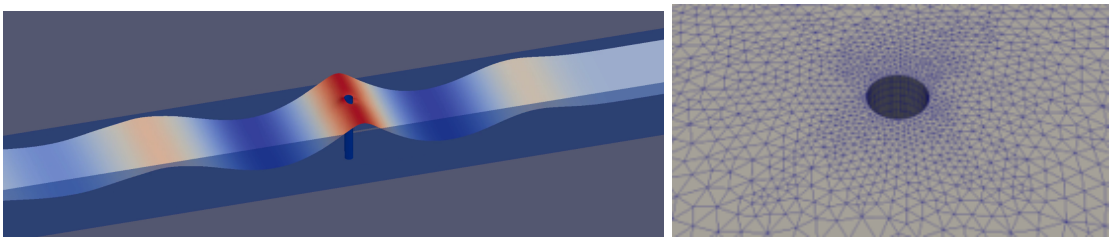

Figure 1: The numerical wave tank model with a circular cylinder. (a) free surface profile; (b) free surface mesh.

3. Results

We consider the bottom-mounted cylinder tested in the Kelvin Tank at the University of Glasgow. The tests were carried out in the lab's 76 m by 4.6 m wave flume with a constant water depth of 1.8 m. The vertical cylinder of diameter 0.315 m was placed at the centre of the tank, 35.315 m away from the wavemaker. A JONSWAP spectrum of peak frequency $f_p = 0.429$ Hz with $\gamma = 3.3$ was used to generate the wave groups. We define the wave group amplitude as $A = \frac{1}{2}H_S$.

3.1. Harmonic forces

We run four times of simulations prescribing the four phases in Eq. (3). Combing the four series of the horizontal wave force on the cylinder, we can separate the force up to fourth order. The separated harmonics in the frequency domain are shown in Figure 2. We see that the extraction is excellent. The first harmonic in solid black line corresponds to the input wave frequency $0.6f_p - 3.0f_p$ with its peak at $1.0f_p$. Some small fifth harmonic can be seen as well. The second and higher harmonics are slightly broadened. We can easily separate the second-order difference component from the fourth harmonic since their frequency ranges are apart enough. The cleanly separated frequency components demonstrate that with careful control of the incident wave phases, which is not a problem for the numerical model but could be difficult in a test, the four-phase method is able to decompose the harmonic loads up to the fourth order.

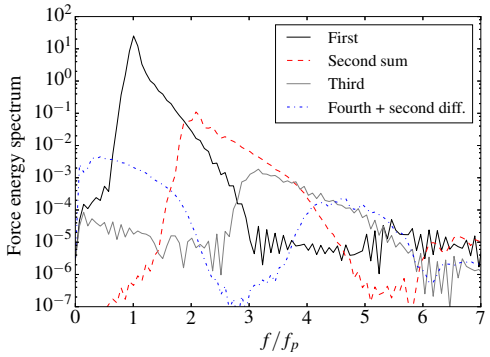

Figure 2: Wave force spectra of separated harmonics in log-scale for $f_p = 0.429$ Hz and $A = 0.11$ m. The horizontal wave force is non-dimensionalized by $\rho g R^2 A$.

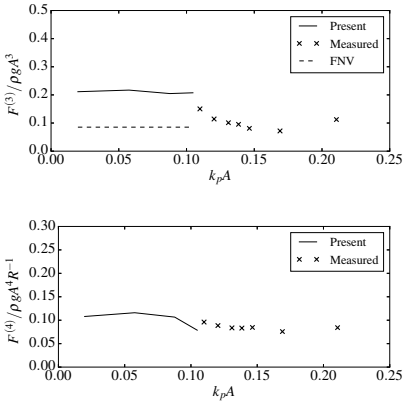

Figure 3: Variation of third and fourth harmonic forces with increasing wave steepness k_pA for $k_pR = 0.129$.

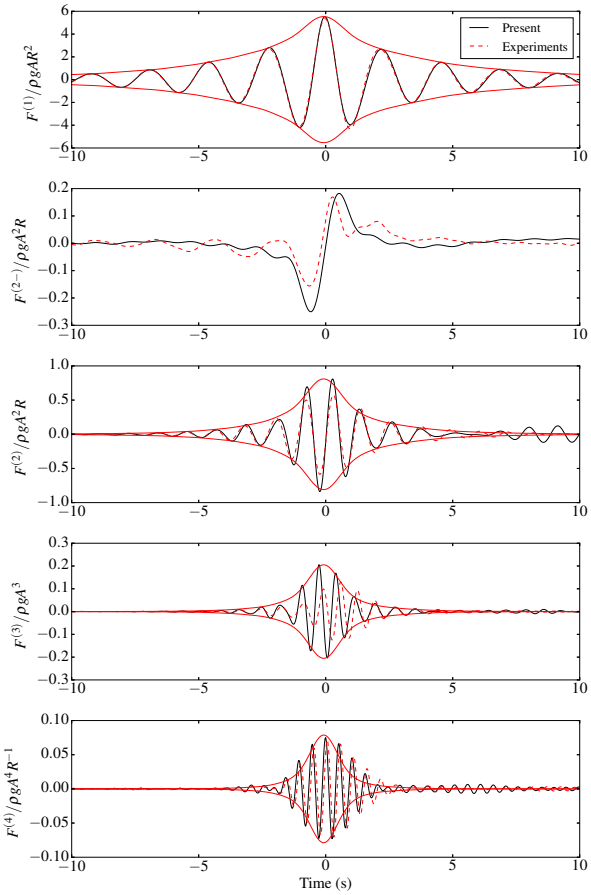

Figure 4: Comparison of decomposed harmonic forces with tests. The forces are non-dimensionalized by $\rho g A^n R^{(3-n)}$. The envelopes of nth harmonics are obtained following the Stokes-type structure assumption.

By inversed FFT, we obtain the time histories of the harmonic forces in Figure 4 where the experimental results from the tests are compared. The time histories are shifted to be focusing at $t = 0.0$ s such that both time series are aligned. The agreement at the first harmonic $F^{(1)}$ is excellent. The red solid line is the envelope of the first harmonic force, computed directly by $F_e^{(1)} = \sqrt{(F^{(1)})^2 + (F_H^{(1)})^2}$ where $F_H^{(1)}$ is the Hilbert transform of $F^{(1)}$. The second harmonic force $F^{(2)}$ shows slight over-prediction than the experiments. For the third harmonic force $F^{(3)}$, there is a slight delay of the peak force; while the fourth harmonic agrees very well. In the plots of the higher harmonic forces, we include the envelope of the time history, the higher harmonic envelope is predicted by scaling the linear envelope $F_e^{(1)}$ to the n th power, $F_e^{(n)} = f_n(F_e^{(1)})^n$. We see that the envelopes agree very well with the time histories of the higher harmonics of the numerical results. This confirms the 'Stokes-type' harmonic structure for the nonlinear loads, and could be useful for estimation of higher harmonic loads from the linear load.

3.2. Harmonic runup

Figure 5 shows the evolution of the first four harmonics of the wave runup upon the cylinder surface. The horizontal axis of each plot is the position angle around the cylinder measuring from the downstream, i.e. $\beta = 180°$ represents the upstream stagnation point. The vertical axis is the time. We see that linear runup shows little variation around the cylinder, since the cylinder is compact and the linear diffraction in the slender body limit. The second harmonic runup is significantly enhanced at the front of the cylinder near the focusing time $t = 25$ s. Mild runup is also observed at the back stagnation point and the cylinder shoulder $\beta = 80°$. The runup around the cylinder becomes more complex at the third and fourth harmonics. More local 'humps' appears around the circumstance and the wave focusing is delayed compared with the first and second harmonics.

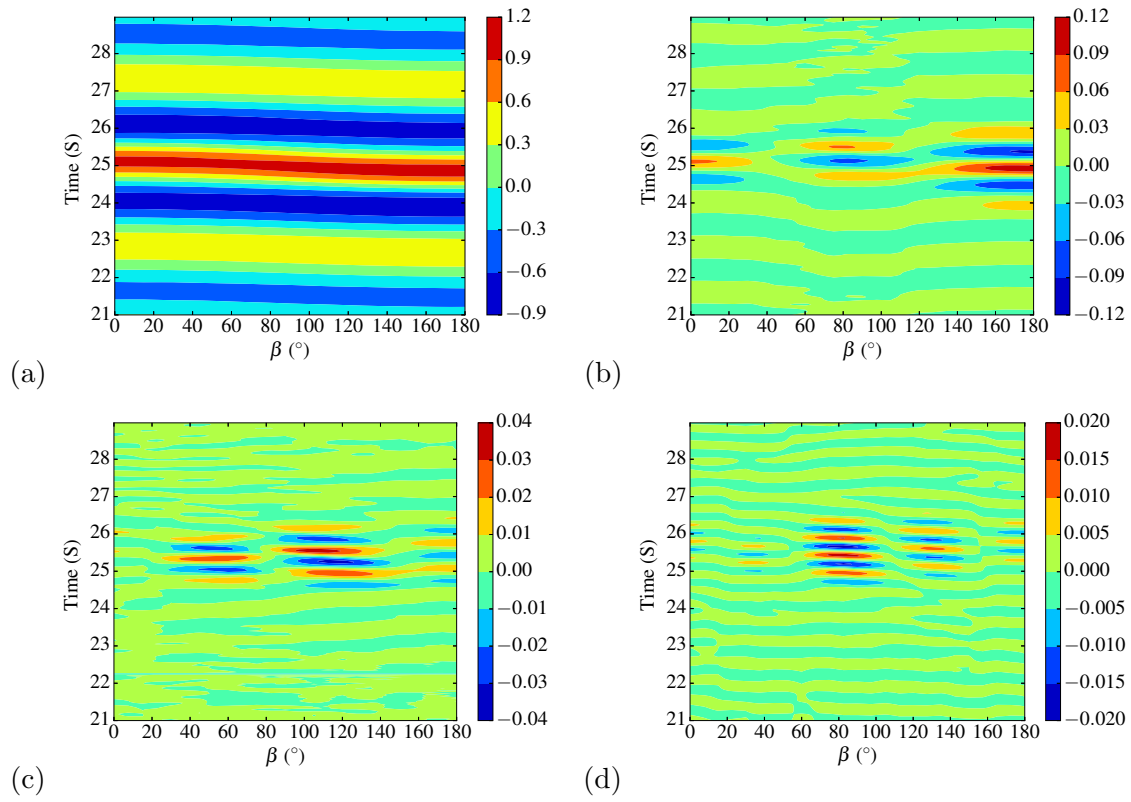

Figure 5: Harmonic runup around the cylinder in the time domain with $\beta = 0°$ the wave direction with $k_pA = 0.074$ and $k_pR = 0.129$. The runup is normalized by A. (a) First; (b) second; (c) third; (d)fourth.

4. Conclusions

A fully nonlinear potential flow numerical wave tank has been extended to simulate focused waves and their interaction with structures. A four-phase manipulation approach has been implemented in the model in order to extract higher harmonic wave elevations and loads. We successfully decompose the harmonic components in the fully nonlinear results and confirm the 'Stokes-type' harmonic structure of loads on a surface-piercing cylinder. Interesting features of higher harmonic wave runup around the cylinder are found.

References

[1] Bai, W. & Eatock Taylor, R. 2006 Higher-order boundary element simulation of fully nonlinear wave radiation by oscillating vertical cylinders. *Applied Ocean Research* **28** (4), 247–265.

[2] Faltinsen, O. M., Newman, J. N. & Vinje, T. 1995 Nonlinear wave loads on a slender vertical cylinder. *Journal of Fluid Mechanics* **289**, 179–198.

[3] Ferrant, P. 1996 Simulation of strongly nonlinear wave generation and wave-body interaction using a 3D MEL model. *Proc. of 21st ONR Symposium on Naval Hydrodynamics, Trondheim* pp. 93–108.

[4] Fitzgerald, C. J., Taylor, P. H., Taylor, R. Eatock Taylor, Grice, J. & Zang, J. 2014 Phase manipulation and the harmonic components of ringing forces on a surface-piercing column. *Proceedings of the Royal Society of London A* **470** (2168).

[5] Malenica, S. & Molin, B. 1995 Third-harmonic wave diffraction by a vertical cylinder. *Journal of Fluid Mechanics* **302**, 203–229.

[6] Rainey, R. C. T. 1995 Slender-body expressions for the wave load on offshore structures. *Proceedings of the Royal Society of London. Series A: Mathematical and Physical Sciences* **450** (1939), 391–416.